AGU PUBLICATIONS

Geophysical Research Letters

RESEARCH LETTER
10.1002/2015GL066255

Key Points:
- Magnetosonic waves at off-equatorial region exhibits harmonic structure
- The multiple frequency spacings are the same as the equatorial proton cyclotron frequency
- Magnetosonic emissions at off-equatorial region originate from multiple equatorial sources

Correspondence to:
Z. Zhima,
zrzm@seis.ac.cn

Citation:
Zhima, Z., L. Chen, H. Fu, J. Cao, R. B. Horne, and G. Reeves (2015), Observations of discrete magnetosonic waves off the magnetic equator, *Geophys. Res. Lett.*, *42*, 9694–9701, doi:10.1002/2015GL066255.

Received 18 SEP 2015
Accepted 10 NOV 2015
Accepted article online 23 NOV 2015
Published online 27 NOV 2015

Observations of discrete magnetosonic waves off the magnetic equator

Zeren Zhima[1,2], Lunjin Chen[2], Huishan Fu[3], Jinbin Cao[3], Richard B. Horne[4], and Geoff Reeves[5]

[1]Institute of Earthquake Science, China Earthquake Administration, Beijing, China, [2]Department of Physics, University of Texas at Dallas, Richardson, Texas, USA, [3]Space Science Institute, School of Astronautics, Beihang University, Beijing, China, [4]British Antarctic Survey, Cambridge, UK, [5]Space Science and Applications Group, Los Alamos National Laboratory, Los Alamos, New Mexico, USA

Abstract Fast mode magnetosonic waves are typically confined close to the magnetic equator and exhibit harmonic structures at multiples of the local, equatorial proton cyclotron frequency. We report observations of magnetosonic waves well off the equator at geomagnetic latitudes from −16.5°to −17.9° and *L* shell ~2.7–4.6. The observed waves exhibit discrete spectral structures with multiple frequency spacings. The predominant frequency spacings are ~6 and 9 Hz, neither of which is equal to the local proton cyclotron frequency. Backward ray tracing simulations show that the feature of multiple frequency spacings is caused by propagation from two spatially narrow equatorial source regions located at $L \approx 4.2$ and 3.7. The equatorial proton cyclotron frequencies at those two locations match the two observed frequency spacings. Our analysis provides the first observations of the harmonic nature of magnetosonic waves well away from the equatorial region and suggests that the propagation from multiple equatorial sources contributes to these off-equatorial magnetosonic emissions with varying frequency spacings.

1. Introduction

Fast mode magnetosonic (MS) waves are linearly polarized electromagnetic emissions, propagating across the ambient magnetic field B_o with the wave vector *k* almost perpendicular to B_o and with frequency ranging from the proton cyclotron frequency (f_{cp}) to the lower hybrid resonant frequency (f_{lh}) [*Russell et al.*, 1970; *Chen and Thorne*, 2012]. The time-frequency spectrograms of MS waves usually display a series of narrow tones spaced at multiples of proton cyclotron frequency [*Perraut et al.*, 1982; *Němec et al.*, 2015a].

MS waves are usually excited with very oblique wave normal angles by a natural instability associated with a ring distribution of energetic protons (over 10 keV) and a ring velocity comparable to or exceeding the local Alfvén speed [*Perraut et al.*, 1982; *Horne et al.*, 2000; *Meredith et al.*, 2008; *Chen et al.*, 2010, 2011]. Previous studies suggest that MS waves can accelerate the energetic electrons (~10 keV) up to relativistic electrons (MeV) on a time scale of ~1 day, which is comparable to the time scale of acceleration by whistler mode chorus waves during storm times [*Horne et al.*, 2007]. Due to their potential to transport energy from ring current ions to radiation belt electrons [e.g., *Jordanova et al.*, 2012], MS waves have recently received increasing attention in radiation belt physics.

Previous studies [*Gurnett*, 1976; *Perraut et al.*, 1982; *Němec et al.*, 2015a] show that MS waves consist of a complex superposition of many harmonic space lines near the magnetic equator. A new study [*Balikhin et al.*, 2015] shows clearly harmonic nature of the equatorial magnetosonic waves at multiple of equatorial proton cyclotron frequencies, confirming that the instability is caused by harmonic cyclotron resonance with proton rings. Recently, Time History of Events and Macroscale Interactions during Substorms satellites, the Van Allen Probes, and Cluster satellites all observed rising tone structures of MS waves [*Fu et al.*, 2014; *Boardsen et al.*, 2014; *Němec et al.*, 2015a], whose formation might be due to nonlinear wave-particle interaction, as is the case with whistler mode chorus and electromagnetic ion cyclotron waves [*Fu et al.*, 2014], or might be due to propagation effects [*Boardsen et al.*, 2014] where the group velocity tends to be slower when the wave frequency approaches to the lower hybrid resonance frequency.

Previous observations [*Russell et al.*, 1970; *Santolík et al.*, 2004; *Hrbáčková et al.*, 2015] show that the majority of MS waves are confined near the magnetic equator region ($|\mathrm{MLAT}| < 5°$), over a broad *L* shell distribution ($2 < L < 9$). Therefore, MS waves are also referred to as equatorial noise emissions [*Russell et al.*, 1970].

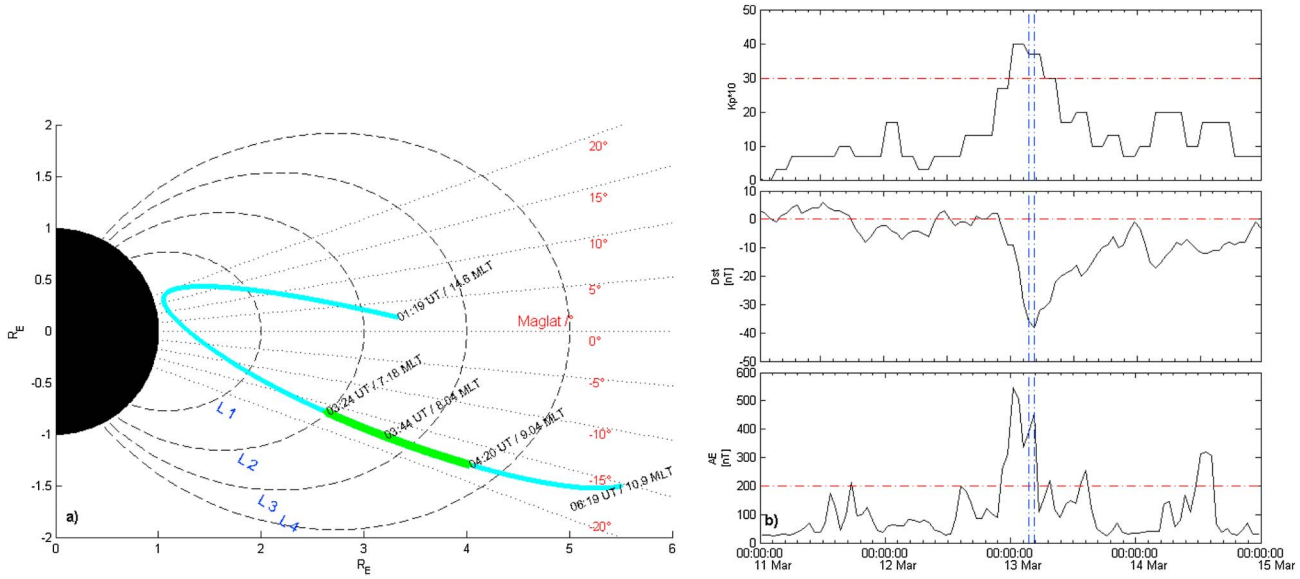

Figure 1. (a) The partial orbit of the Van Allen Probe A on 13 March 2014. The cyan line represents the orbit from 01:19 to 06:19 UT, and the overlapping green line marks the region where MS waves are observed. The dotted lines display the magnetic latitude lines, and the dashed curves denote the magnetic field lines. (b) Time series of *Kp*, *Dst*, and *AE* index over four days period from 11 to 15 March, the two vertical dashed lines mark the time interval of the MS wave event of interest.

However, only a few studies [*Gurnett*, 1976; *André et al*., 2002; *Tsurutani et al*., 2014] suggest that sometimes MS waves also can exist at off-equatorial region ($|\mathrm{MLAT}| > 5°$). Based on the observations of Polar satellite, *Tsurutani et al*. [2014] recently reported that MS waves can exist at high latitudes as far as 60° away from the equator; however, the wave intensity of those high-latitude MS waves is weak, and also, the harmonic structures of MS waves were not clearly found. In this letter we will present spectral and polarization properties of a MS wave event that exhibits clear discrete spectral structures well away from the equatorial region (MLAT ~ 17°). Backward ray tracing simulations give evidence that the off-equatorial emissions with varying frequency spacings originate from multiple equatorial sources.

2. Observations

An event of interest was measured on 13 March 2014 by the probe A of the twin Van Allen Probes (formerly known as the Radiation Belt Storm Probes). The Van Allen Probes have highly elliptical, low-inclination orbits with a perigee ~1.1 R_E and an apogee ~5.9 R_E [*Mauk et al*., 2013], and are ideally suited to study the characteristics of magnetosonic waves. In this study, the data from the Electric and Magnetic Field Instrument Suite and Integrated Science (EMFISIS) [*Kletzing et al*., 2013], the Electric Field and Waves Instrument (EFM) [*Wygant et al*., 2013], the Helium, Oxygen, Proton, and Electron (HOPE) instrument [*Funsten et al*., 2013] of the Energetic Particle Composition and Thermal Plasma Suite [*Spence et al*., 2013] are used. EMFISIS consists of a fluxgate magnetometer, a Waveform Frequency Receiver (WFR), and a High-Frequency Receiver. The WFR measures six components of electric field and magnetic field for waves with frequency range from 10 Hz to 12 kHz, and WFR also provides wave propagation parameters which are computed onboard by the Singular Value Decomposition (SVD) method [*Santolík et al*., 2003]. The HOPE measures the Helium, Oxygen, Proton, and Electron with energy range from ~1 eV to ~50 keV.

Figure 1a shows the orbit of the Van Allen Probe A from 01:19 to 06:19 UT on 13 March 2014. The overlapping green line demonstrates the off-equatorial region (MLAT ~ −16.5° to −17.9°) where MS waves are observed from 03:24 to 4:20 UT (7.18 to 9.04 MLT) at *L* shell from ~2.7 to 4.6. The geomagnetic activity during the period MS waves are observed is shown in Figure 1b, suggesting that a moderate storm occurred with *Dst* index reaching below~ −38 nT, *AE* over 455 nT, and *Kp* over 3. The variation of *AE* index indicates that this storm is a complex set of substorm activities. The magnetosonic waves are detected at the morning sector a few hours after the initiation of the storm, which is about the time scale for energetic ions to drift all the way around from the nightside, through the duskside and the noon to the morningside.

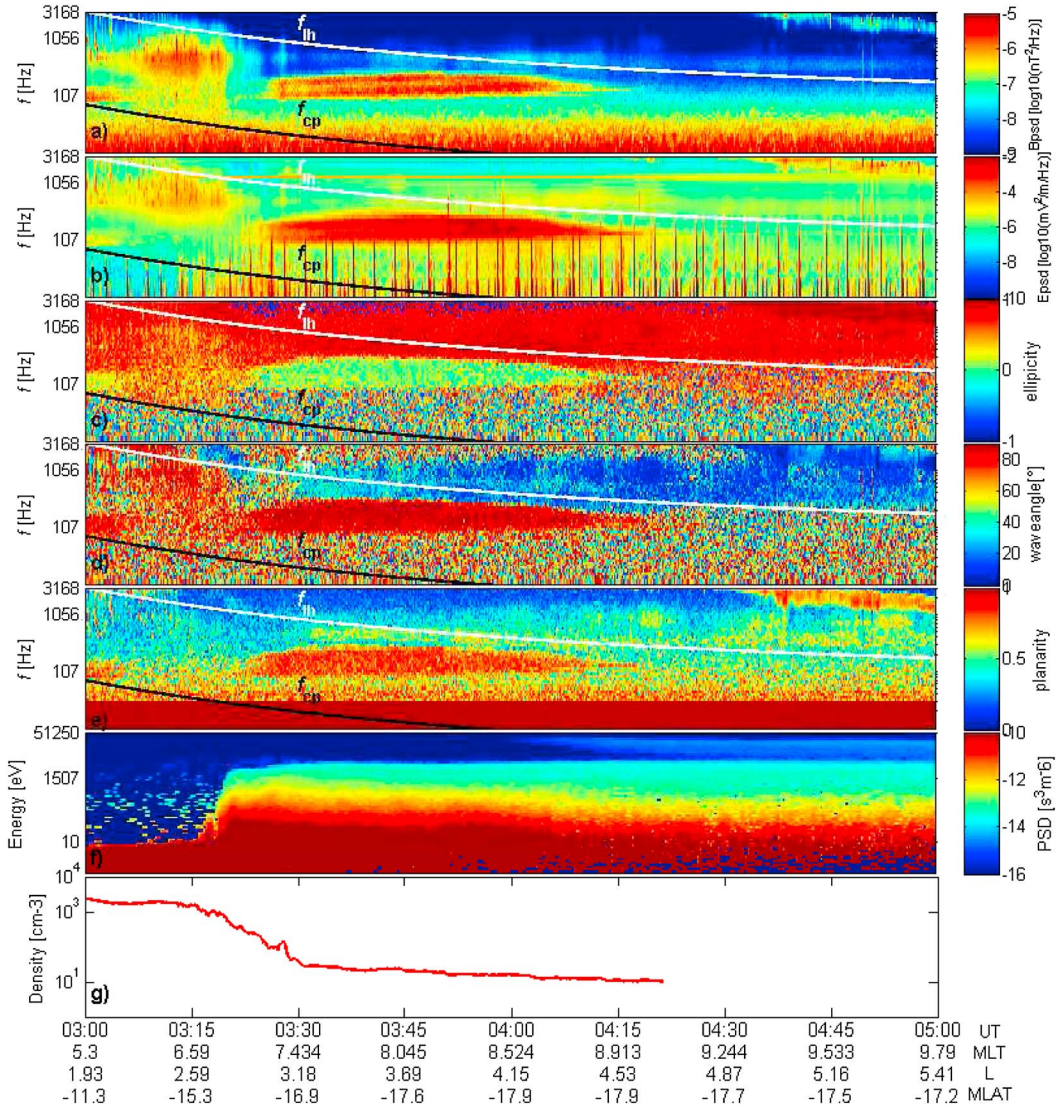

Figure 2. An overview of the off-equatorial MS waves observed by the Van Allen Probe A from 03:24 to 04:20 UT on 13 March 2014. (a) The power spectral density of the magnetic field (B_{psd}); (b) the power spectral density in the electric field (E_{psd}). The white and black solid curves represent the lower hybrid resonant frequency (f_{lh}) and the proton cyclotron frequency (f_{cp}), respectively. The wave propagation parameters are (c) the ellipticity, (d) the wave normal angle, and (e) the planarity of polarization. (f) The proton phase space densities (PSD) over the energy range from ~1 eV to ~50 keV; (g) the plasma density inferred from spacecraft potential. Data are displayed as a function of universal time (UT), magnetic local time (MLT), *L* shell, and geomagnetic latitude (MLAT), respectively.

Figure 2 shows an overview of this off-equatorial MS wave event. As seen in Figures 2a–2b, which show the power spectral density of magnetic (B_{psd}) and electric (E_{psd}) components respectively, an enhancement of wave intensity both in the electric and magnetic field are observed at 03:24 to 04:20 UT, suggesting that these emissions are electromagnetic. Clearly, the enhanced waves are observed mainly between the proton gyrofrequency f_{cp} (black curves) and the lower hybrid resonant frequency f_{lh} (white curves), which is usually the frequency range of MS waves. The wave propagation parameters computed by the SVD method [*Santolík et al.*, 2003] are shown in Figures 2c–2e. The ellipticity of these electromagnetic emissions is near 0, which means that the emissions are linearly polarized (Figure 2c); the wave normal angle (Figure 2d) is close to 90°, which indicates that these waves are nearly perpendicular to the ambient magnetic field; the planarity is about 1 (Figure 2e), suggesting that the waves are polarized nearly in a single plane [*Santolík et al.*, 2003]. Such wave propagation and polarization properties generally satisfy the definition of MS waves [*Russell et al.*, 1970; *Santolík et al.*, 2004; *Tsurutani et al.*, 2014]. It is

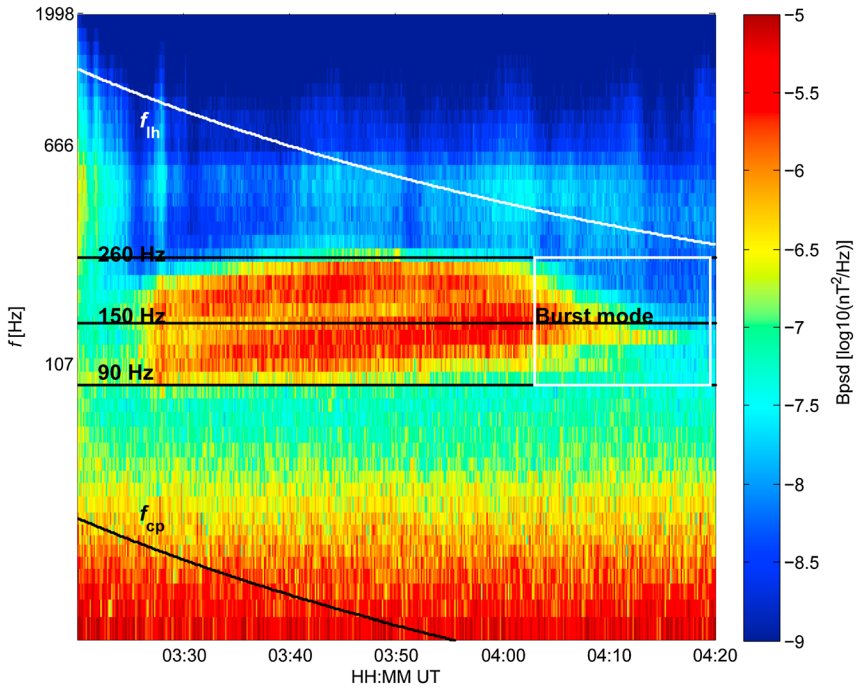

Figure 3. A close-up view of the off-equatorial MS waves at magnetic field component. The white and black solid curves represent the lower hybrid resonant frequency (f_{lh}) and the proton cyclotron frequency (f_{cp}), respectively. The white rectangle represents that the burst mode observation of wave instrument onboard are triggered.

also interesting to note that two bands of magnetosonic waves are observed just before 03:30 UT and merge to a single band near 04:00 UT.

In addition, the electron density estimated from the spacecraft potential [*Wygant et al.*, 2013] is plotted in Figure 2g, showing the existence of a gradual plasmapause where the electron density decreases from ~1.5×10^3 cm^{-3} (at $L \sim 2.59$) to 26 cm^{-3} (at $L \sim 3.18$). Clearly, this off-equatorial MS event mainly occurs outside the plasmapause ($L > 2.7$) after ~03:15 UT and seems not to be able to penetrate into the plasmasphere. The phase space density (PSD) at the pitch angle 90°for the ions with energy from ~1 eV to ~50 keV measured from the HOPE instrument [*Funsten et al.*, 2013] is shown in Figure 2f. It can be seen that there is no pronounced ion ring in the heart of the intense waves in Figure 2f, suggesting that local proton harmonic gyroresonance instability is not operative at this latitude (~17°) of MS wave event, but it is possible that a ring distribution could still be present at the magnetic equator. Additionally, the waves in Figure 2 appear almost constant in frequency and do not vary with f_{lh} or $f_{cp,}$ also suggesting that they are not produced locally.

A close-up view of these off-equatorial MS waves at magnetic component is shown in Figure 3. It is clear that this MS wave event mainly occurred from 03:24 UT to 04:20 UT, within the frequency range of 90–260 Hz (covered by nine frequency channels of EMFISIS), and the intensity mostly peaks at frequency ~150 Hz. The root-mean-square of wave amplitude over the frequency range from 90 Hz to 260 Hz, ~22 pT, is weaker than the average amplitude (50 pT) obtained by *Ma et al.* [2013].

The white rectangular in Figure 3 represents the burst mode observation of the wave instrument onboard, and the burst mode observation lasted over 15 min from 04:03:25 UT to 04:18:01 UT. A total of 12 sets of waveform samples of electric and magnetic vectors are recorded, with sampling rate 33,140 Hz and each lasting a period of ~6 s. The first four waveform samples from 04:03:25 UT to 04:03:49 UT are almost seamlessly connected, which provides ~24 s of continuous waveform in total. Those waveform samples at the first 24 s are examined in order to obtain high-resolution frequency spectral properties. First, the waveform samples are calibrated using the calibration method provided by instrument team (https://emfisis.physics.uiowa.edu/Waveform_Calibration). Second, fast Fourier transforms with time window of 3 s are applied to each component. Thus, the resulting frequency resolution is $\triangle f = 0.33$ Hz. Finally, the magnetic field power spectral density, computed as the sum of power spectral density of three magnetic components, is displayed in Figure 4a as a function of both frequency

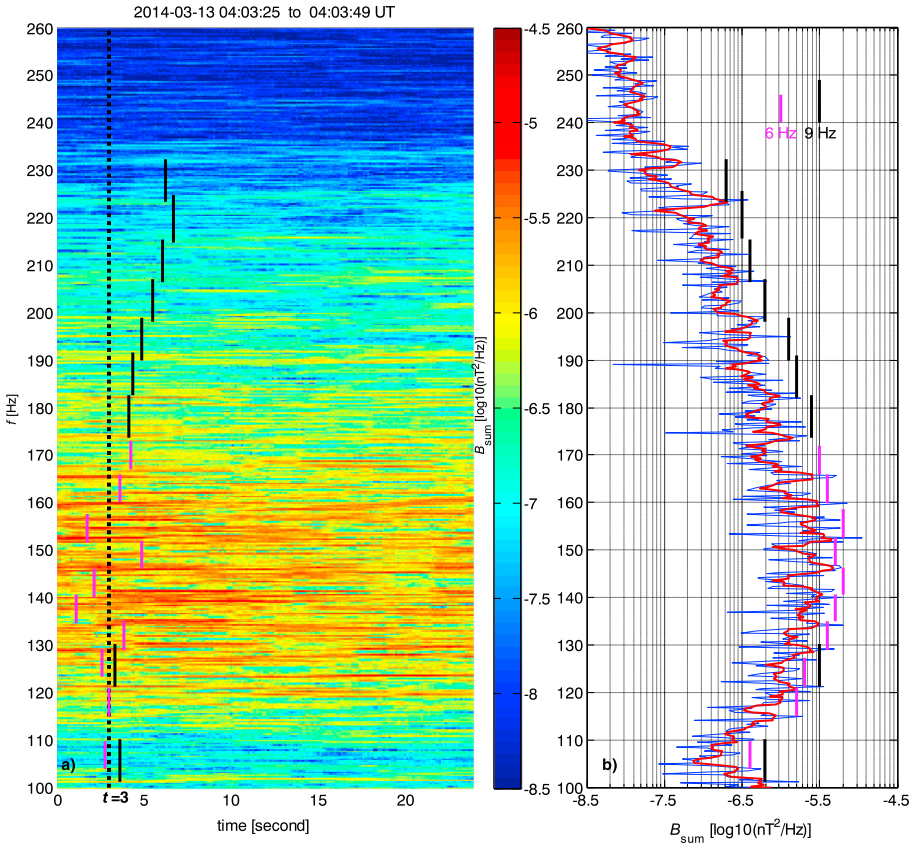

Figure 4. The detailed frequency spectral properties of the off-equatorial MS waves from burst mode observation. (a) The total wave spectral density of three magnetic components recorded from 04:03:25 to 04:03:49 UT at frequency band from 100 to 260 Hz; (b) the total wave spectral density at a given time (04:03:28 UT) along the profile of vertical dashed line ($t = 3$) in Figure 4a. The pink and black bar represents the scale of 6 Hz and 9 Hz, respectively.

and time. The magnetic field power spectral density as a function of frequency for a given time 04:03:28 UT (indicated by the vertical dashed line in Figure 4a) is shown in Figure 4b. The red line in Figure 4b represents the moving average of the power spectral density over five neighboring frequency bins.

It can be seen in Figure 4 that the MS emissions consist of many discrete lines instead of being a broadband noise. There exists multiple frequency separation and the accurate identification of the frequency separation is hindered by the finite frequency broadness (about a fraction of hertz) and slight variation of discrete frequency with time. Nonetheless, two frequency separations, ~6 Hz and ~9 Hz, are clearly identified by eye inspection. The pink and black bars as an aid to the visualization, denoting the scale of 6 Hz and 9 Hz, respectively, are added in Figure 4b. It can be seen that the 6 Hz frequency separation is seen over the frequency from 130 to 165 Hz, while the 9 Hz frequency separation is clear from 173 to 232 Hz. Similar discrete lines are also present in the electric components (not shown).

The proton cyclotron frequencies both at equator and off-equatorial regions (MLAT ~ −16.5° to −17.9°) are computed. Specifically, the proton cyclotron frequency at equator region with L shell from 3.8 to 4.2 (see 03:50 to 04:03 UT in Figure 2) varies from ~6 to 9 Hz, while for the same time interval of interest, the local proton cyclotron frequency ranges from ~9 to 12 Hz. It can be seen that the frequency spacings in Figure 4 are close to the equatorial proton cyclotron frequency. This feature implies that the source region of the off-equatorial MS waves is near magnetic equator region.

3. Discussion

The observation of different frequency spacings implies that these MS waves at the off-equatorial region might originate from multiple equatorial sources having different proton gyrofrequencies. Using ray tracing

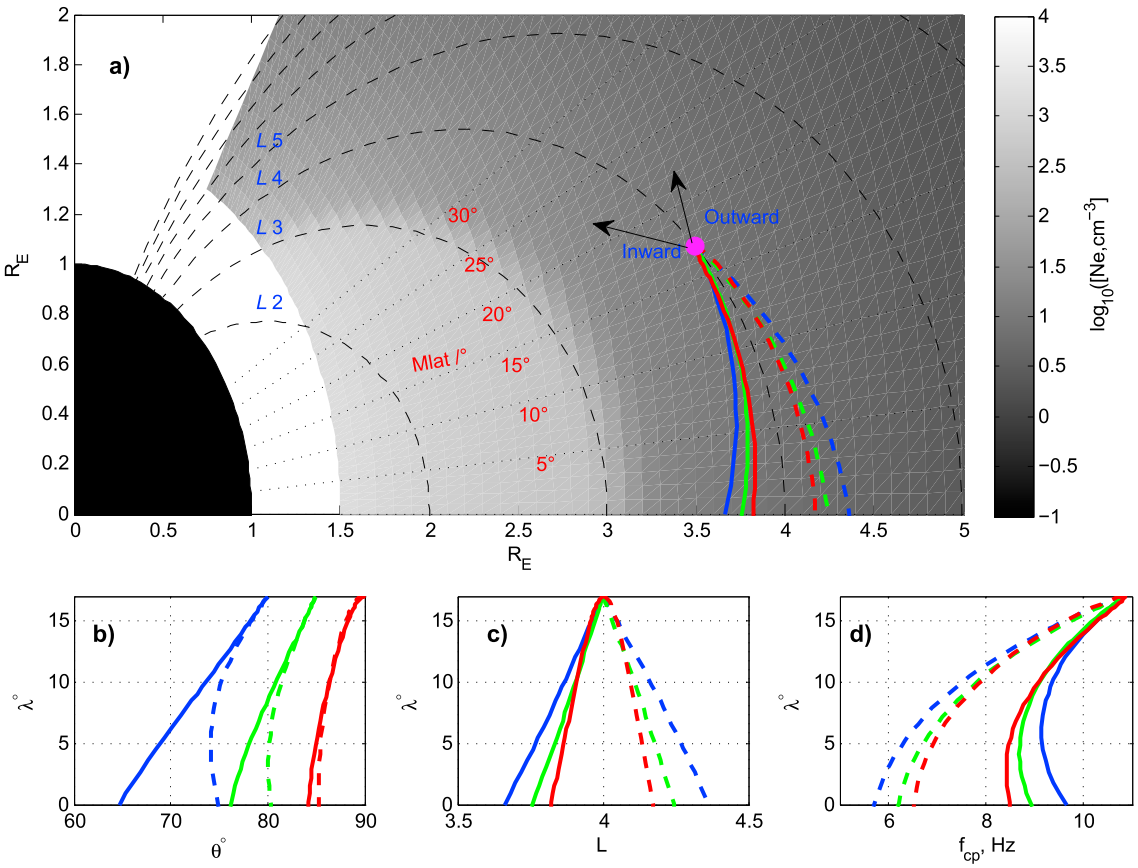

Figure 5. Backward ray tracing simulation for rays with a given frequency 160 Hz launched from MLAT = ±17°at $L = 4$ (filled magenta circle). (a) Ray paths of MS waves with wave normal angles pointing outward (inward) denoted by solid (dashed) colored lines, where colors represent different values of wave normal angles at that location, 80° (blue), 85°(green), and 90°(red). The black dashed lines represent the dipole magnetic fields. The gray color represents the distribution of plasma density; the variations of wave normal angle (b) θ, (c) L shell, and (d) local proton gyrofrequency along the ray paths; λ denotes geomagnetic latitude.

code HOTRAY [*Horne*, 1989], a well-established model for waves in magnetized plasma, we perform backward ray tracing to examine propagation of magnetosonic waves and to identify the source location. Here a dipole magnetic field and a modified diffusive equilibrium described in *Bortnik et al.* [2011] are adopted, and the plasmapause is set to be $L = 3.2$ based on the plasma density observation in Figure 2g.

Figure 5 shows the results of backward ray tracing simulation for rays with a given frequency of 160 Hz launched from off-equatorial region with MLAT = ±17° at L shell = 4. Although the waves are observed in the Southern Hemisphere, we perform ray tracing in the Northern Hemisphere for symmetries in both plasma density and dipole magnetic field about the equator. Because of the observed obliqueness of magnetosonic waves at this latitude (Figure 2d), rays are launched with three wave normal angles ($\theta = 80°$, 85°, and 90°) and each ray has both wave vectors pointing toward smaller L and toward larger L. A total of six rays are traced, and the ray path are shown in Figure 5a, where the blue, green, and red lines represent wave normal angles $\theta = 80°$, 85°, and 90°, respectively, and the dashed (solid) lines represent launched wave vectors pointing toward smaller (larger) L. Figures 5b–5d display the variations of wave normal angle θ, L shell, and local proton gyrofrequency along the ray paths as a function of geomagnetic latitude λ.

As seen in Figure 5, the oblique emissions at this relatively high-latitude region can originate from two spatially narrow equatorial regions in the same meridional plane. One equatorial source region locates at $L \approx 3.75$ with equatorial proton gyrofrequency about ~6 Hz, while the other one locates at L near 4.25 with equatorial proton gyrofrequency of ~9 Hz. The two gyrofrequencies are consistent with harmonic frequency spacings in the observed emissions at the off-equatorial region (see Figure 4). This gives evidence that the off-equatorial emissions of varying frequency spacings originate from multiple equatorial sources. One may also place a constraint on the oblique wave normal angle at the equator, which is usually $\theta > 80°$ for

the proton ring instability. Then such constraint will make the two spatial extensions narrower, because the three rays in Figure 5b (dashed and solid blue rays, and the solid green ray) have $\theta < 80°$ at the equator and thus violate the constraint.

One may also note that there is no prominent proton ring distribution at the off-equatorial region where the harmonic magnetosonic waves are observed (Figure 2g). This may be due to the fact that those protons of equatorial pitch angle near 90° cannot access latitudes as high as 17°, where electrons of equatorial pitch angle at least less than 56° are available (assuming dipole magnetic field). Nonetheless, weak proton ring distribution (see energy bands around 20–50 keV in Figure 2f) starts to appear as the satellite moves toward the magnetic equator (after 4:15 UT).

There might be two possibilities of observing discrete MS emission outside the source region. One possibility is that the source region is localized over a narrow range of L. Assuming that plasma waves are emitted at harmonics of the local proton gyrofrequency, one can estimate an upper limit of the L range to avoid merging into a continuum, that is, the L range corresponding to $N\Delta f_{cp} \sim f_{cp}$, where N is the proton cyclotron harmonic number of interests, For the case of $L = 4$ and a typical value of $N = 10$, this condition yields an upper limit of the L range $\Delta L \sim 0.075$ under the assumption of a dipole magnetic field. This possibility is less likely according to previous estimation of $\Delta L > \sim 0.1$ [e.g., *Němec et al.*, 2015b]. A second possibility is that the discrete structures at relatively high latitude can be retained due to propagation. Propagation characteristics constrain the origin of the off-equatorial MS wave emissions from spatially separated and localized regions inside the equatorial source region, instead of from the entire source region. As a consequence, the emissions have not yet merged into a continuum and discrete nature can be preserved off the equator. According to ray tracing simulation and consistent observations of the two clear harmonic spacings, the second possibility is likely the case.

We would like to provide three notes here. First, the observed wave amplitude (~22 pT) at this off-equatorial event is weak, which might be due to wave damping along the propagation [e.g., *Horne et al.*, 2000]. Since there are no magnetosonic wave observations in the equatorial source at the same time, an accurate damping estimation is not possible. However, using the average wave amplitude 50 pT suggested by *Ma et al.* [2013], a rather rough estimation of wave convective damping rate can be made: $\sim \ln(50\,\text{pT}/22\,\text{pT})/(D_s) \approx 1.1 \times 10^{-7}\,\text{m}^{-1}$. Here D_s represents the distance traveled by the waves, which can be approximated as $D_s = L \cdot \text{MLAT} \cdot R_E$. In this event MS waves are detected at $L \sim 4$, MLAT ~ 17°, and here Earth radii $R_E = 6371 \times 10^3$ m. Second, we also checked directional information through Poynting flux analysis (not shown). It is found that dominant component of Poynting flux lies in the plane perpendicular to the background magnetic field. The direction on the perpendicular plane does not show robust signatures to draw a meaningful conclusion. This might be due to multiple coincident emissions from different source regions, which blur the direction of individual emissions. Third, the magnetosonic waves at the off-equatorial region place an upper bound on wave normal angles of equatorial waves through proton instability. The higher the latitude, the smaller is the wave normal angle at the equator. This might be useful for obtaining the wave normal angle information, when there is no burst mode data available or when the wave normal angle within a few degree from 90° cannot be resolved through available waveform data.

4. Conclusions

On 13 March 2014, the Van Allen Probe A observed enhanced electromagnetic emissions from the proton cyclotron frequency to the lower hybrid resonant frequency at the off-equatorial region ($-16.5° < \text{MLAT} < -17.9°$) over L shell ~2.7–4.6. Observations show that such off-equatorial electromagnetic waves are linearly polarized and propagate nearly perpendicular to the ambient magnetic field, indicating that these off-equatorial electromagnetic emissions are magnetosonic waves. Detailed spectral properties of magnetosonic waves show that the off-equatorial magnetosonic waves exhibit discrete spectral lines and there exist multiples of frequency spacings, including ~6 and 9 Hz, which are the same as the equatorial proton cyclotron frequencies at $L = 4.2$ and 3.7, respectively. Our analysis first reveals the discrete nature of magnetosonic waves at the off-equatorial region and the existence of multiple harmonic spacings. We simulate the propagating process of MS waves to study why MS waves exhibit different harmonic frequency spacing at off-equatorial region based on the observational parameters. Results indicate that the oblique MS emissions at the off-equatorial region may originate from two spatially separated narrow equatorial regions in the same meridional plane.

Acknowledgments
We acknowledge NASA Goddard Space Flight Center Space Physics Data Facility (http://cdaweb.gsfc.nasa.gov/istp_public/) for the use of observation data from the Van Allen Probes (EMFISIS, EFM, WFR, ECT, and HOPE). This work was supported by the ISTCP 2014DFR21280, the NSFC grant 41204136, 41274166, and 973 Program grant 2011CB811404, the Fundamental Research Funds for earthquake research 2014IES010203. Lunjin Chen acknowledge the support of NSF grant AGS 1405041. The research leading to these results has received funding from the European Union Seventh Framework Programme (FP7/2007-2013) under grant agreement 606716 SPACESTORM.

References

André, R., F. Lefeuvre, F. Simonet, and U. S. Inan (2002), A first approach to model the low-frequency wave activity in the plasmasphere, *Ann. Geophys.*, *20*(7), 981–996.

Balikhin, M. A., Y. Y. Shprits, S. N. Walker, L. Chen, N. Cornilleau-Wehrlin, I. Dandouras, O. Santolik, C. Carr, K. H. Yearby, and B. Weiss (2015), Observations of discrete harmonics emerging from equatorial noise, *Nat. Commun.*, *6*, doi:10.1038/ncomms8703.

Boardsen, S. A., G. B. Hospodarsky, C. A. Kletzing, R. F. Pfaff, W. S. Kurth, J. R. Wygant, and E. A. MacDonald (2014), Van Allen Probe observations of periodic rising frequencies of the fast magnetosonic mode, *Geophys. Res. Lett.*, *41*, 8161–8168, doi:10.1002/2014GL062020.

Bortnik, J., L. Chen, W. Li, R. M. Thorne, and R. B. Horne (2011), Modeling the evolution of chorus waves into plasmaspheric hiss, *J. Geophys. Res.*, *116*, A08221, doi:10.1029/2011JA016499.

Chen, L., and R. M. Thorne (2012), Perpendicular propagation of magnetosonic waves, *Geophys. Res. Lett.*, *39*, L14102, doi:10.1029/2012GL052485.

Chen, L., R. M. Thorne, V. K. Jordanova, and R. B. Horne (2010), Global simulation of magnetosonic wave instability in the storm time magnetosphere, *J. Geophys. Res.*, *115*, A11222, doi:10.1029/2010JA015707.

Chen, L., R. M. Thorne, V. K. Jordanova, M. F. Thomsen, and R. B. Horne (2011), Magnetosonic wave instability analysis for proton ring distributions observed by the LANL magnetospheric plasma analyzer, *J. Geophys. Res.*, *116*, A03223, doi:10.1029/2010JA016068.

Fu, H. S., J. B. Cao, Z. Zhima, Y. V. Khotyaintsev, V. Angelopoulos, and O. Santolík (2014), First observation of rising-tone magnetosonic waves, *Geophys. Res. Lett.*, *41*, 7419–7426, doi:10.1002/2014GL061867.

Funsten, H. O., et al. (2013), Helium, Oxygen, Proton, and Electron (HOPE) mass spectrometer for the radiation belt storm probes mission, *Space Sci. Rev.*, *179*(1–4), 423–484, doi:10.1007/s11214-013-9968-7.

Gurnett, D. A. (1976), Plasma wave interactions with energetic ions near the magnetic equator, *J. Geophys. Res.*, *81*(16), 2765–2770, doi:10.1029/JA081i016p02765.

Horne, R. (1989), Path-integrated growth of electrostatic waves: The generation of terrestrial myriametric radiation, *J. Geophys. Res.*, *94*(A7), 8895–8909, doi:10.1029/JA094iA07p08895.

Horne, R. B., G. V. Wheeler, and H. S. C. K. Alleyne (2000), Proton and electron heating by radially propagating fast magnetosonic waves, *J. Geophys. Res.*, *105*(A12), 27,597–27,610, doi:10.1029/2000JA000018.

Horne, R. B., R. M. Thorne, S. A. Glauert, N. P. Meredith, D. Pokhotelov, and O. Santolík (2007), Electron acceleration in the Van Allen radiation belts by fast magnetosonic waves, *Geophys. Res. Lett.*, *34*, L17107, doi:10.1029/2007GL030267.

Hrbáčková, Z., O. Santolík, F. Němec, E. Macúšová, and N. Cornilleau-Wehrlin (2015), Systematic analysis of occurrence of equatorial noise emissions using 10 years of data from the Cluster mission, *J. Geophys. Res. Space Physics*, *120*, 1007–1021, doi:10.1002/2014JA020268.

Jordanova, V. K., D. T. Welling, S. G. Zaharia, L. Chen, and R. M. Thorne (2012), Modeling ring current ion and electron dynamics and plasma instabilities during a high-speed stream driven storm, *J. Geophys. Res.*, *117*, A00L08, doi:10.1029/2011JA017433.

Kletzing, C. A., et al. (2013), The Electric and Magnetic Field Instrument Suite and Integrated Science (EMFISIS) on RBSP, *Space Sci. Rev.*, *179*(1–4), 127–181, doi:10.1007/s11214-013-9993-6.

Ma, Q., W. Li, R. M. Thorne, and V. Angelopoulos (2013), Global distribution of equatorial magnetosonic waves observed by THEMIS, *Geophys. Res. Lett.*, *40*, 1895–1901, doi:10.1002/grl.50434.

Mauk, B. H., N. J. Fox, S. G. Kanekal, R. L. Kessel, D. G. Sibeck, and A. Ukhorskiy (2013), Science objectives and rationale for the radiation belt storm probes mission, *Space Sci. Rev.*, *179*(1–4), 3–27, doi:10.1007/s11214-012-9908-y.

Meredith, N. P., R. B. Horne, and R. R. Anderson (2008), Survey of magnetosonic waves and proton ring distributions in the Earth's inner magnetosphere, *J. Geophys. Res.*, *113*, A06213, doi:10.1029/2007JA012975.

Němec, F., O. Santolík, Z. Hrbáčková, J. S. Pickett, and N. Cornilleau-Wehrlin (2015a), Equatorial noise emissions with quasiperiodic modulation of wave intensity, *J. Geophys. Res. Space Physics*, *120*, 2649–2661, doi:10.1002/2014JA020816.

Němec, F., O. Santolík, Z. Hrbáčková, and N. Cornilleau-Wehrlin (2015b), Intensities and spatiotemporal variability of equatorial noise emissions observed by the Cluster spacecraft, *J. Geophys. Res. Space Physics*, *120*, 1620–1632, doi:10.1002/2014JA020814.

Perraut, S., A. Roux, P. Robert, R. Gendrin, J.-A. Sauvaud, J.-M. Bosqued, G. Kremser, and A. Korth (1982), A systematic study of ULF waves above FH+ from GEOS 1 and 2 measurements and their relationships with proton ring distributions, *J. Geophys. Res.*, *87*(A8), 6219–6236, doi:10.1029/JA087iA08p06219.

Russell, C. T., R. E. Holzer, and E. J. Smith (1970), OGO 3 observations of ELF noise in the magnetosphere: 2. The nature of the equatorial noise, *J. Geophys. Res.*, *75*(4), 755–768, doi:10.1029/JA075i004p00755.

Santolík, O., M. Parrot, and F. Lefeuvre (2003), Singular value decomposition methods for wave propagation analysis, *Radio Sci.*, *38*(1), 1010, doi:10.1029/2000RS002523.

Santolík, O., F. Němec, K. Gereová, E. Macúšová, Y. de Conchy, and N. Cornilleau-Wehrlin (2004), Systematic analysis of equatorial noise below the lower hybrid frequency, *Ann. Geophys.*, *22*(7), 2587–2595, doi:10.5194/angeo-22-2587-2004.

Spence, H. E., et al. (2013), Science goals and overview of the Radiation Belt Storm Probes (RBSP) Energetic Particle, Composition, and Thermal Plasma (ECT) suite on NASA's Van Allen probes mission, *Space Sci. Rev.*, *179*(1–4), 311–336, doi:10.1007/s11214-013-0007-5.

Tsurutani, B. T., B. J. Falkowski, J. S. Pickett, O. P. Verkhoglyadova, O. Santolik, and G. S. Lakhina (2014), Extremely intense ELF magnetosonic waves: A survey of polar observations, *J. Geophys. Res. Space Physics*, *119*, 964–977, doi:10.1002/2013JA019284.

Wygant, J. R., et al. (2013), The electric field and waves instruments on the radiation belt storm probes mission, *Space Sci. Rev.*, *179*(1–4), 183–220, doi:10.1007/s11214-013-0013-7.